Contents lists available at ScienceDirect

Electrochimica Acta

Oxide-coated silicon nanowire array capacitor electrodes in room temperature ionic liquid

L. Qiao[a], A. Shougee[b], T. Albrecht[a,1,*], K. Fobelets[b]

[a] Department of Chemistry, Imperial College London, Exhibition Road, SW7 2AZ London, UK
[b] Electrical and Electronic Engineering Department, Imperial College London, Exhibition Road, SW7 2BT London, UK

ABSTRACT

Improved performance of Si nanowire arrays for capacitor electrodes in ionic liquid [Bmim][NTf$_2$], is obtained by spin-on-doping the nanowires followed by hot, concentrated nitric acid oxidation. n- and p-type Si nanowire arrays are fabricated via a 2-step metal-assisted chemical etch process to increase the effective surface area. Spin-on-doping increases the doping density of the nanowires, enhancing the current by a factor of more than 3. The well-controlled HNO$_3$ oxidation defines a thin, dense oxide layer on the Si nanowires increasing chemical stability, both expanding the electrochemical window and increasing the current further by a factor >2. Specific capacitances of $238\,\mu F\,cm^{-2}$ ($\sim0.4\,F\,g^{-1}$, $159\,mF\,cm^{-3}$) and $404\,\mu F\,cm^{-2}$ ($\sim0.7\,F\,g^{-1}$, $269\,mF\,cm^{-3}$) are obtained for n- and p-type Si nanowire arrays, respectively.

© 2016 Elsevier Ltd. All rights reserved.

1. Introduction

To improve the capacitance value of electrolytic or double-layer capacitors, the use of nanostructured materials is an area that is currently being explored. In double-layer capacitors, the charge separation is obtained between an electrode and a liquid electrolyte with mobile ions rather than a solid dielectric [1,2].

Silicon nanowires (SiNWs) are being investigated in this context [3–7], since amongst other things, the use of Si may facilitate monolithic integration of the capacitor with CMOS circuits via the application of techniques developed for Si-based MEMS (micro electro-mechanical systems). SiNWs grown by vapour-liquid-solid chemical vapour deposition (VLS-CVD) have shown particular promise, with reported areal electrode capacitances for n-type and p-type [5] Si of $34\,\mu F\,cm^{-2}$ and $46\,\mu F\,cm^{-2}$, respectively. Increasing the NW density of 3–5 μm long SiNWs 160 times (to $8\times10^9\,NWs\,cm^{-2}$) was shown to improve the areal capacitance from $5.2\,\mu F\,cm^{-2}$ to $36.7\,\mu F\,cm^{-2}$ [7]. All of these values were obtained with a 3-electrode set-up, as in this work.

However, a key limitation of Si-based electrodes is the reactivity of Si with the electrolyte that limits the use of uncoated SiNWs as capacitor electrodes. Surface modification may thus be required for further performance enhancement. To this end, improved electrode stability was achieved by CVD coating the SiNWs with e.g. graphene [8], diamond [9] and MnO$_2$ nanoflakes [10], compared to bare SiNWs [4,5,7] with reported capacitance values of C $\sim9\,F\,g^{-1}$, $0.1\,mF\,cm^{-2}$ and $13\,mF\,cm^{-2}$ ($51\,F\,g^{-1}$), respectively. In comparison, three-dimensional structures of graphene, diamond foam and MnO$_2$ are reported to show specific capacitance values of C $\sim250\,F\,g^{-1}$ [11], $0.598\,mF\,cm^{-2}$ [12] and $214\,F\,g^{-1}$ [13], respectively. The MnO$_2$ based electrodes show higher specific capacitance values, since MnO$_2$ as a pseudocapacitive material supports Faradaic charge storage.

On the other hand, undesired Faradaic reactions may also be suppressed by coating the Si surface with a thin, but highly insulating oxide layer. To this end, electrochemical surface oxidation of VLS-CVD grown SiNWs in an ionic liquid (IL) (1-ethyl-3-methylimidazolium bis(trifluoromethylsulfonyl)imide) was employed in [6], thus avoiding vacuum techniques or high temperature oxidation steps. This greatly enhanced the electrochemical window, from 1.3 V to 4 V. In principle, ILs are a very promising electrolyte medium, since some of them feature very wide electrochemical stability windows (6 V and larger), are environmentally more benign than many organic solvents, and have very low vapour pressure. However, they can be relatively viscous, thus limiting their electric conductivity, and hygroscopic. High water content tends to decrease the electrochemical window, due to Faradaic reactions from solution and on the electrode

* Corresponding author.
  E-mail address: t.albrecht@imperial.ac.uk (T. Albrecht).
1 ISE member.

surface, and is thus undesired in the context of energy storage (even though some water content can also decrease the viscosity and thus increase the conductivity) [14]. From an application point of view, the use of ultra-dry ILs may be difficult, so this aspect requires some attention when assessing the true potential of ILs in this context.

In the present study, we use a metal-assisted chemical etching (MACE) fabrication method for SiNW electrodes in supercapacitor applications, in order to obtain high-density arrays of SiNWs [8,15–19] with a high surface-to-volume ratio, crystalline core and direct connection to the Si substrate electrode. Since the doping density of the Si for etching crystalline NWs is relatively low, the SiNW arrays (SiNWAs) were doped using spin-on-doping (SOD) to increase conductivity. We then use hot, concentrated HNO_3 as an alternative method to oxidise the surface of the NWs, leading to further improvement of the electrode performance (compared to electrochemical oxidation performed previously). Both SOD and HNO_3 oxidation are simple, well-controllable procedures, and in the absence of vacuum techniques or high temperature processes, the overall fabrication strategy for Si-based supercapacitor electrodes presented here is thus feasible as a post-process step in Si CMOS.

We investigate the performance of the SiNWAs in [Bmim][NTf$_2$] (1-Butyl-3-methylimidazolium bis(trifluoromethylsulfonyl)imide) IL, due to its favourable electrochemical properties and the lack of free fluoride (which may adversely affect the stability of the electrode surface) [20]. We compare the performance of SiNWAs with and without SOD, and with and without thin HNO_3-grown SiO_2 layer, in order to quantify the improvement in performance.

2. Experimental

2.1. Fabrication of SiNWA

SiNWAs were fabricated by a two-step MACE process: (1) nucleation of Ag onto Si in a solution of 0.005 M $AgNO_3$ and 5 M HF, and (2) etching in a solution of 0.1 M H_2O_2 and 4.9 M HF [21]. The Ag film that nucleates on the samples during MACE is removed in concentrated HNO_3. After etching, the samples were cleaned in DI water and dried using a dry-air gun. Both n- and p-type samples were fabricated with NW lengths of $\sim$15 μm, average diameter of 150 nm, and a density of $\sim$10^9 NWs cm^{-2}. Since MACE on highly doped Si results in porous or brittle NWs, we etch wires in $\rho \approx 0.02\,\Omega$ cm Si. Samples were subsequently doped with boron (p-type) and phosphorus (n-type) with a SOD process to improve electrical conductivity. SOD (BDC1-2000 and PDC1-2000 from Futurrex Inc.) was carried out by spinning the dopant solution onto the SiNWA at 2500 rpm for 40 s. This was followed by a low temperature bake at 200 °C to evaporate the solvent, then a high temperature anneal (800–1000 °C for 1 min) for diffusion of dopant atoms. The resistivity after SOD of the p- and n-type SiNWA is $\rho \approx 0.003\,\Omega$ cm and $\rho \approx 0.014\,\Omega$ cm, based on thermo-electric power measurements [21]. The same process was carried out on the back of the wafer. After stripping any residual existing surface oxides in diluted HF, a thin, well-defined oxide layer was grown on the NW surface by immersion in heated (90–120 °C) concentrated HNO_3 (67% wt.) for 10–15 min. The thickness of the oxide layer is estimated to be between 1–2 nm based on reports of similar one-step oxidation processes [22,23]. XPS characterisation confirms an increased 'Si in SiO_2' content, compared to before oxidation. A low resistance contact was formed on the bulk side of the sample by first stripping the SiO_2 layer from the bulk via plasma etching (200 W for 10 min), followed by thermal evaporation of a $\sim$100 nm Al layer and subsequent annealing at 200 °C for 1 min in Ar gas. The wet chemical processes result in bunching of the tops of the NWs that can be minimised via different processes

[24]. Wetting of the SiNWA by the [Bmim][NTf$_2$] IL was investigated with a droplet test [25]. The immediate spreading of IL on the SiNWA surface with negligible contact angle demonstrated high wettability thus maximizing the overall contact area.

2.2. Electrochemical characterisation

Electrochemical characterisation was conducted in the dark at room temperature at different scan rates, using a three-electrode configuration controlled by a potentiostat (CH Instruments, CH760C). The SiNWA was placed in a custom-built electrochemical cell to bring the IL in contact with the SiNWA whilst insulating it from the Al back contact on the Si substrate. SiNWAs with a substrate area of 2.8 cm^2 were used as working electrode, Pt and Ag wires as counter and reference electrodes, respectively. The electrochemical window, ΔV, has been determined by cyclic voltammetry (CV), namely from the potential range without significant current increase ($I_{max} < 3 \times I_{mid-window}$). The electrochemical window of [Bmim][NTf$_2$] was estimated to be 2.05 V using a Au electrode (IL water content: $\sim$110 ppm, Karl-Fischer titration) [26]. With the main focus of our study on new electrode materials and fabrication methodologies, no effort was made to reduce the water content further at this stage. The capacitance of the SiNWAs was evaluated using CV, electrochemical impedance spectroscopy (EIS), and galvanostatic charge/discharge curves.

3. Results and discussion

3.1. Influence of SOD

The conductivity of the SiNWA electrode is a factor that affects the electrode performance and can be increased by SOD, cf. §2.1 [21]. n- and p-type SiNWAs with and without modification by SOD were compared by CV (Fig. 1). For n-SiNWA, the current density increases by a factor of $\sim$3 for the SOD sample compared to the non-treated sample due to a decrease in electrode resistivity. The electrochemical window also increases from $\sim$0.55 V to $\sim$0.65 V, potentially due to a thin SOD-related residual oxide layer that increases the chemical stability of the SiNWs. For p-SiNWA, the current density for the SOD sample also increases, by a factor >5. However, an additional redox peak appears in the centre of the electrochemical window. With repeated cycling (50$\times$), this redox feature of the highly doped sample becomes more prominent and then remains constant. Its position in relation to the electrochemical window does not change (the overall shift is attributed to instabilities in the potential of the Ag reference electrode).

Fig. 2 a) displays the SEM cross sectional image and top view of the p-SiNWA after SOD. The top inset shows that the SiNWs surface is porous, which increases the effective surface area of the electrode. The top view inset of Fig. 2a shows that a residual layer is present on the top surface of the wires before oxidation. This layer can be associated with a boron rich layer [27], and albeit being potentially highly conductive, it can also restrict access of the IL to the NWs (hence decreasing the actual surface area). This layer may be contributing to the redox peak seen in the CV of the p-type sample post-SOD, and is less apparent after oxidation (Fig. 2b).

3.2. Influence of HNO_3 oxidation

Fig. 3 compares the CV measurements of 5 different working electrodes, with and without surface oxidation (surface area Si substrate = 2.8 cm^2): Au (orange), bulk Si (green), SOD treated SiNWA (blue), electro-oxidised SOD SiNWA (red) and HNO_3-oxidised SOD SiNWA (black). Si and SiNWA exhibit reduced electrochemical windows compared to Au, which suggests that ΔV
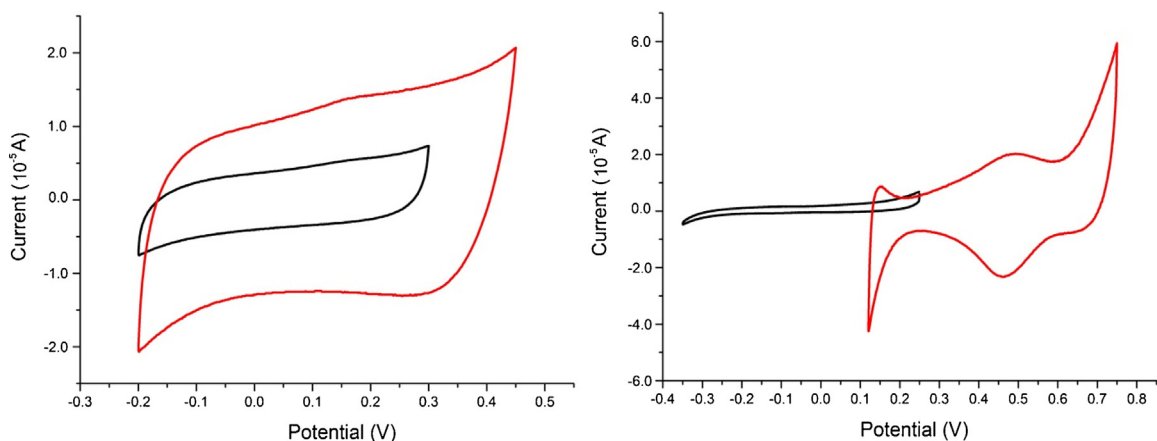
Fig. 1. CV in [Bmim][NTf₂] of SOD (red) and non-SOD (black) SiNWA. Left: n-type; right: p-type (scan rate: 50 mV/s). (For interpretation of the references to colour in this figure legend, the reader is referred to the web version of this article.)
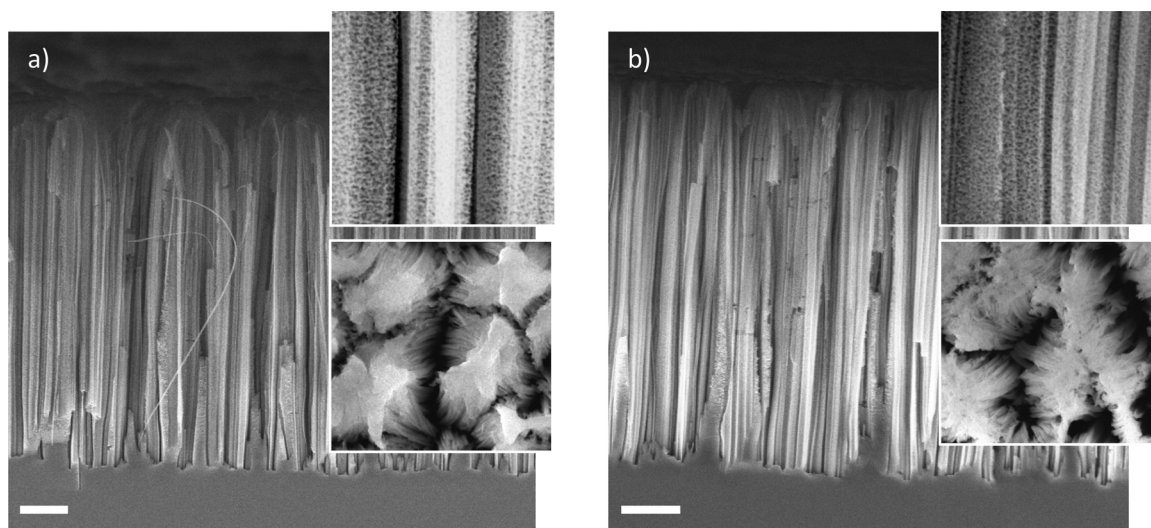
Fig. 2. SEM cross-sections of SiNWA without (a) and with (b) oxidation. Insets are zoomed-in, showing surface porosity (top right, cross section) and SiNW bunching (bottom right, top view). Scale bars are 2 μm.
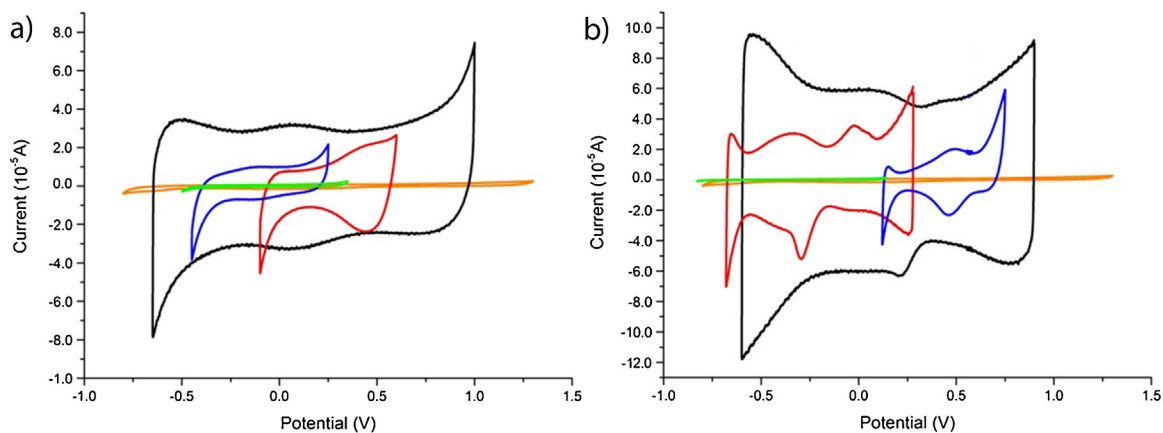
Fig. 3. CV measurements in [Bmim][NTf₂] of 5 working electrodes (Si surface area = 2.8 cm²; Au: ∼0.13 cm²): Au (orange), bulk Si (green), SOD treated SiNWA (blue), electro-oxidised SiNWA (red) and HNO₃-oxidised SiNWA (black). (a) n-type (HNO₃-oxidised at 120 °C), (b) p-type (HNO₃-oxidised at 90 °C). Scan rate: 50 mV/s. (For interpretation of the references to colour in this figure legend and text, the reader is referred to the web version of this article.)

is limited by electrochemical reactions specific to the Si/SiNWA electrode surface. However, the increased effective surface area by nano-structuring of bulk Si into SiNWA, in conjunction with SOD-enhanced conductivity, leads to a ten-fold increase in current and thus capacitance for both n- and p-type SiNWA over bulk Si. Electrochemical oxidation reported in [6] showed marginal improvement of current density and electrochemical window in the n-type, while a significant improvement occurred in the p-type sample (more than doubling the current density and extending the electrochemical window by ~0.35 V).

We found an even larger improvement in performance after HNO_3 oxidation and the concomitant growth of a thin, high-density oxide layer on the Si surface. In both n- and p-type samples, current densities increase at least by a factor of 3, and the electrochemical windows were more than doubled, with $\Delta V \approx 1.7$ V and 1.5 V for n- and p-type, respectively compared to 2.05 V with Au). The reason for the increased operational potential window is relatively straightforward and due to the enhanced chemical stability of the oxidised SiNWA in the IL, thus blocking (undesired) Faradaic reactions. The origin of the increase in capacitance after oxide coating is perhaps less obvious. In a simple plane-parallel capacitor model, an increased separation between the electrolyte ions and the charges on the electrode surface (e.g. due to the oxide film) should lead to a decrease in the capacitance. However, SEM imaging shown in Fig. 2 provided some evidence that surface oxidation leads to the removal of the boron-rich top layer, thus facilitating access of ions to the Si nanostructure, Fig. 2 a,b bottom insets. This would lead to an increase in the effective surface area of the electrode and hence the observed capacitance. Other factors may also have contributed, such as increased wettability of the electrode with oxidation or changes in the local dielectric constant. At present, we are unable to quantify these different factors.

The areal capacitance can be extracted from the CV curves of Fig. 3 by [6]:

$$C_{CV} = \frac{i}{dV/dt} \times \frac{1}{A} \qquad (1)$$

where i is the current, dV/dt is the scan rate and A is the projected surface area.

CV measurements at different scan rates show a linear dependence of the current on scan rate, in the absence of Faradaic side reactions at potentials of E = 0.4 V (n-type) and 0.32 V (p-type), Fig. 4 a), Fig. 4a. The slopes are 0.61×10^{-3} As/V (for n-type) and 1.13×10^{-3} As/V (for p-type), yielding capacitance values of 216.3 ± 5.1 μF cm^{-2} and 404.0 ± 9.5 μF cm^{-2}, respectively (nominal surface area: 2.8 cm^2). Compared to previous work on SiNWAs, these values are found to be higher than those reported in [4–7].

The galvanostatic charge/discharge (GCD) curves in Fig. 4b) are symmetrical and show a small sudden potential drop at the beginning of the discharge. This IR drop has been associated to the resistance of the electrolytes and the inner resistance of electrolyte ion migration in the porous electrode material [28]. Capacitances extracted from GCD curves using eq. (1) are in the same region as the values from CV, with $C_{GCD} = 180$ μF cm^{-2} for n-type and 290 μF cm^{-2} for p-type (taking dV/dt inclusive of IR drop rather than from the slope). This also yields near identical power densities of 291 μW cm^{-2} for n-type and 293 μW cm^{-2} for p-type, based on these capacitance values.

In order to further support the extracted (effective) capacitance values, EIS measurements were done in a frequency range between $0.1 Hz < f < 100 kHz$. The Nyquist plots of both n- and p-type oxidised SiNWAs are given in Fig. 5. Circuit fitting was carried out on the Nyquist data using a simplified Randles circuit to model the electrode, along with an additional RC component to represent the Al on Si metal contact, Fig. 6.
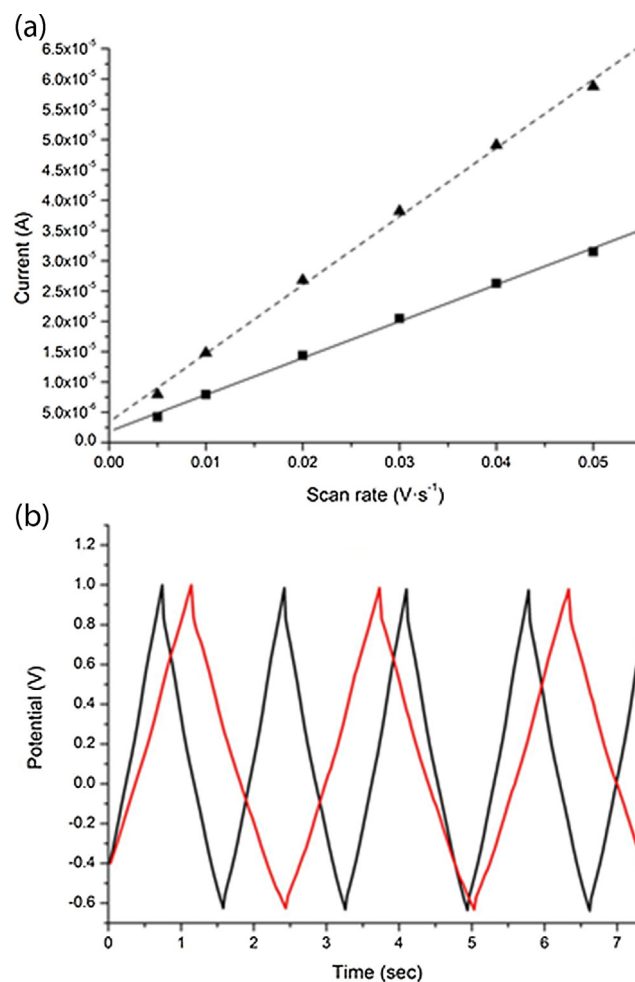
Fig. 4. (a) Capacitive current as a function of scan ratefor HNO_3-oxidized n-type (squares) and p-type SiNWAs (triangles), inc. linear fits (r^2 = 0.998 for both), determined at a substrate potential of 0.4 V for n-type and 0.32 V for p-type. The slopes are 0.61×10^{-3} As/V (for n-type) and 1.13×10^{-3} As/V (for p-type), yielding capacitance values of 216.3 ± 5.1 μF cm^{-2} and 404.0 ± 9.5 μF cm^{-2}, respectively (nominal surface area: 2.8 cm^2). The intercepts are negligible, compared to the overall change in the current. (b) Galvanostatic charge/discharge curves at 1 mA, for HNO_3-oxidized n-type (black) and p-type SiNWAs (red) The slopes of the ascending and descending branches are constant and proportional to the capacitance, eq. (1) (see text for further details). (For interpretation of the references to colour in this figure legend, the reader is referred to the web version of this article.)

Double layer capacitance values extracted from the fitting yield similar values to those obtained from CV, with $C_{EIS} = 238$ μF cm^{-2} for n-type and $C_{EIS} = 379$ μF cm^{-2} for p-type.

A comparison of values extracted from the three different methods, namely CV, GCD and EIS is shown in Table 1. The CV and EIS values are in close agreement, with the GCD extracted values being somewhat lower, albeit within the same order of magnitude and with similar p-type to n-type ratio. This is presumably due to the IR drop in the GCD measurement resulting in a higher effective dV/dt, and thus the values can be taken as an underestimation of capacitance.

Therefore, areal capacitance values, including estimates for volumetric and gravimetric capacitances, are demonstrated to be up to 238 μF cm^{-2} (159 mF cm^{-3}, ~0.4 F g^{-1}) for n-type and 404 μF cm^{-2} (269 mF cm^{-3}, ~0.7 F g^{-1}) for p-type. Volumetric values are obtained on the basis of a 15 μm SiNW length. Gravimetric estimates are based on an approximate density of ~10^9 NW cm^{-2}, an average SiNW diameter of 150 nm and a material density of 2.32 g cm^{-3} (as per Si).
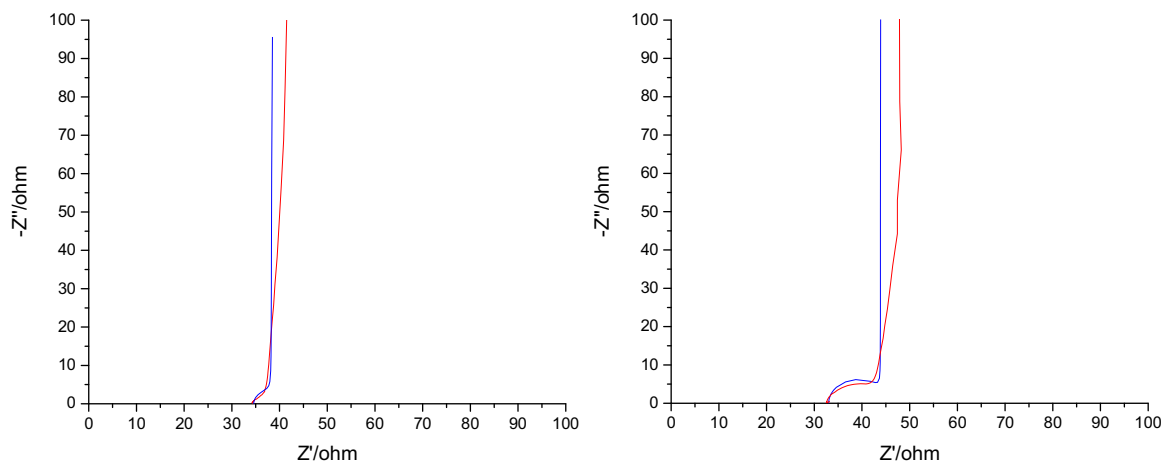
Fig. 5. Nyquist plots (red) and fitting (blue) of n-type (left) and p-type (right) HNO$_3$ oxidised SiNWAs.
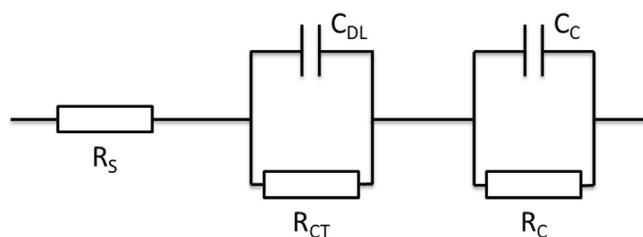

Fig. 6. Equivalent circuit model for Nyquist fitting. R$_S$, R$_{CT}$ and C$_{DL}$ are uncompensated solution resistance, charge transfer resistance and double layer capacitance, respectively. R$_C$ and C$_C$ represent the Al on Si contact that provides the working electrode connection for 3-electrode measurements.

Table 1
Areal capacitance comparison of HNO$_3$ oxidised SiNWAs.

Sample	C_{CV} (μF cm^{-2})	C_{GCD} (μF cm^{-2})	C_{EIS} (μF cm^{-2})
n-type	216	180	238
p-type	404	290	379

4. Conclusion

We have studied the use of n- and p-type SiNWAs as working electrodes for electrolytic capacitors in [Bmim][NTf$_2$] IL. The MACE-etched SiNWAs enlarge the effective surface area and enable direct electrode contact (to Si). A SOD process was applied to reduce the resistance of the NWs in the array, more than tripling the current density of the electrodes. The HNO$_3$-generated SiO$_2$ coating on the SiNWs increased the systems' electrochemical window to 1.7 V and 1.5 V, and also increased the current densities, leading to significantly improved areal capacitances of up to 238 μF cm^{-2} ($\sim$0.4 F g^{-1}, 159 mF cm^{-3}) and 404 μF cm^{-2} ($\sim$0.7 F g^{-1}, 269 mF cm^{-3}) for n-type and p-type SiNWAs, respectively. These values are almost a factor of 10 higher than experimental values using a 3-electrode measurement set-up previously reported for CVD grown SiNW electrolytic capacitor electrodes [5–7]. Based on the mass estimate for our best performing system, we calculate a specific power density of 651 W kg^{-1} and specific energy density of 0.23 Wh kg^{-1}, placing these capacitors well within the range of other electrochemical capacitors on the Ragone plot [29]. The advantage to the presented technique is the low cost process and avoiding the use of vacuum equipment and high temperatures, making the monolithic integration of these structures into microelectronic chips feasible. Further improvements in performance may be achieved by preventing bunching of the NWs in the arrays (in order to increase the surface area accessible to the electrolyte), by increasing the doping density via multiple SOD steps and by reducing the water content in the IL, to increase the operational potential window further.

References

[1] P. Simon, Y. Gogotsi, Materials for electrochemical capacitors, Nature Materials 7 (11) (2008) 845–854.
[2] M. Winter, R.J. Brodd, What are batteries, fuel cells, and supercapacitors? Chemical reviews 104 (10) (2004) 4245–4270.
[3] J.W. Choi, J. McDonough, S. Jeong, J.S. Yoo, C.K. Chan, Y. Cui, Stepwise nanopore evolution in one-dimensional nanostructures, Nano Letters 10 (4) (2010) 1409–1413.
[4] F. Thissandier, N. Pauc, T. Brousse, P. Gentile, S. Sadki, Micro-ultracapacitors with highly doped silicon nanowires electrodes, Nanoscale Research Letters 8 (1) (2013) 1–5.
[5] F. Thissandier, A. Le Comte, O. Crosnier, P. Gentile, G. Bidan, E. Hadji, T. Brousse, S. Sadki, Highly doped silicon nanowires based electrodes for micro-electrochemical capacitor applications, Electrochemistry Communications 25 (2012) 109–111.
[6] N. Berton, M. Brachet, F. Thissandier, J. Le Bideau, P. Gentile, G. Bidan, T. Brousse, S. Sadki, Wide-voltage-window silicon nanowire electrodes for micro-supercapacitors via electrochemical surface oxidation in ionic liquid electrolyte, Electrochemistry Communications 41 (2014) 31–34.
[7] F. Thissandier, L. Dupré, P. Gentile, T. Brousse, G. Bidan, D. Buttard, S. Sadki, Ultra-dense and highly doped SiNWs for micro-supercapacitors electrodes, Electrochimica Acta 117 (2014) 159–163.
[8] S. Chatterjee, R. Carter, L. Oakes, W.R. Erwin, R. Bardhan, C.L. Pint, Electrochemical and Corrosion Stability of Nanostructured Silicon by Graphene Coatings: Toward High Power Porous Silicon Supercapacitors, J Phys. Chem. C 118 (2014) 10893–10902.
[9] F. Gao, G. Lewes-Malandrakis, M.T. Wolfer, W. Müller-Sebert, P. Gentile, D. Aradilla, T. Schubert, C.E. Nebel, Diamond-coated silicon wires for supercapacitor applications in ionic liquids, Diamond and Related Materials 51 (2015) 1–6.
[10] D.P. Dubal, D. Aradilla, G. Bidan, P. Gentile, T.J.S. Schubert, J. Wimberg, S. Sadki, P. Gomez-Romero, 3D hierarchical assembly of ultrathin MnO$_2$ nanoflakes on silicon nanowires for high performance micro-supercapacitors in Li-doped ionic liquid, Scientific Reports 5 (2015) 09771.

[11] C. Li, X. Zhang, K. Wang, H.-T. Zhang, X.-Z. Sun, Y.-W. Ma, Three dimensional graphene networks for supercapacitor electrode materials, New Carbon Materials 30 (3) (2015) 193–206.

[12] F. Gao, M.T. Wolfer, C.E. Nebel, Highly porous diamond foam as a thin-film micro-supercapacitor material, Carbon 80 (2014) 833–840.

[13] P. Wang, Y.-J. Zhao, L.-X. Wen, J.-F. Chen, Z.-G. Lei, Ultrasound-Microwave-Assisted Synthesis of MnO Supercapacitor Electrode Materials, Ind Eng. Chem. Res. 53 (2014) 20116–20123.

[14] M. Armand, F. Endres, D.R. MacFarlane, H. Ohno, B. Scrosati, Ionic-liquid materials for the electrochemical challenges of the future, Nature materials 8 (8) (2009) 621–629.

[15] Z. Huang, N. Geyer, P. Werner, J. de Boor, U. Gösele, Metal-assisted chemical etching of silicon: a review, Advanced materials 23 (2) (2011) 285–308.

[16] S.K. Srivastava, D. Kumar, S.W. Schmitt, K.N. Sood, S.H. Christiansen, P.K. Singh, Large area fabrication of vertical silicon nanowire arrays by silver-assisted single-step chemical etching and their formation kinetics, Nanotechnology 25 (17) (2014) 175601.

[17] Y. Hu, K.Q. Peng, Z. Qiao, X. Huang, F.Q. Zhang, R.N. Sun, X.M. Meng, S.T. Lee, Metal-Catalyzed Electroless Etching of Silicon in Aerated HF/H2O Vapor for Facile Fabrication of Silicon Nanostructures, Nano letters 14 (8) (2014) 4212–4219.

[18] W.K. Choi, T.H. Liew, M.K. Dawood, H.I. Smith, C.V. Thompson, M.H. Hong, Synthesis of silicon nanowires and nanofin arrays using interference lithography and catalytic etching, Nano letters 8 (11) (2008) 3799–3802.

[19] J. de Boor, N. Geyer, J.V. Witterman, U. Gösele, V. Schmidt, Sub-100 nm silicon nanowires by laser interference lithography and metal-assisted etching, Nanotechnology 21 (9) (2010) 095302.

[20] J.C. Flake, M.M. Rieger, G.M. Schmid, P.A. Kohl, Electrochemical etching of silicon in nonaqueous electrolytes containing hydrogen fluoride or fluoroborate, Journal of The Electrochemical Society 146 (5) (1999) 1960–1965.

[21] B. Xu, K. Fobelets, Spin-on-doping for output power improvement of silicon nanowire array based thermoelectric power generators, Journal of Applied Physics 115 (21) (2014) 214306.

[22] Asuha, S.S. Im, M. Tanaka, S. Imai, M. Takahashi, H. Kobayashi, Formation of 10-30 nm SiO 2/Si structure with a uniform thickness at ∼120 °C by nitric acid oxidation method, Surface Science 600 (12) (2006) 2523–2527.

[23] N.E. Grant, K.R. McIntosh, Passivation of a (100) silicon surface by silicon dioxide grown in nitric acid, Electron Device Letters, IEEE 30 (9) (2009) 922–924.

[24] C. Li, K. Fobelets, C. Liu, C. Xue, B. Cheng, Q. Wang, Ag-assisted lateral etching of Si nanowires and its application to nanowire transfer, Applied Physics Letters 103 (18) (2013) 183102.

[25] Y. Yuan, T.R. Lee, Contact angle and wetting properties. In Surface science techniques, Springer, Berlin Heidelberg, 2013, pp. 3–34.

[26] P. Hapiot, C. Lagrost, Electrochemical reactivity in room-temperature ionic liquids, Chemical Reviews 108 (7) (2008) 2238–2264.

[27] S. Ingole, P. Aella, P. Manandhar, S.B. Chikkannanavar, E.A. Akhadov, D.J. Smith, S.T. Picraux, Ex situ doping of silicon nanowires with boron, J. Appl. Phys. 103 (2008) 104302.

[28] C.-T. Hsieh, H. Teng, Influence of oxygen treatment on electric double-layer capacitance of activated carbon, Carbon 40 (2002) 667–674.

[29] P. Sharma, T.S. Bhatti, A review on electrochemical double-layer capacitors, Energy Conversion and Management 51 (12) (2010) 2901–2912.